Available online at www.sciencedirect.com
SCIENCE DIRECT®
Microelectronic Engineering 83 (2006) 528–535
MICROELECTRONIC ENGINEERING
www.elsevier.com/locate/mee

S-parameters-based high speed signal characterization of Al interconnect on low-*k* hydrogen silsesquioxane-Si substrate

Chia-Cheng Ho [a,1], Bi-Shiou Chiou [a,b,*]

[a] *Department of Electronics Engineering and Institute of Electronics, P.O. Box 83, Engineering Building IV, 1001 Ta Hsueh Road, Hsinchu, Taiwan*
[b] *Innovative Packaging Research Center, National Chiao Tung University, Hsinchu, Taiwan*

Received 19 August 2005; received in revised form 19 November 2005; accepted 12 December 2005
Available online 10 January 2006

Abstract

The International Technology Roadmap for Semiconductors (ITRS) predicts that by 2010 over one billion transistors will be integrated into one chip [Semiconductor Industry Associations, International Technology Roadmap for Semiconductors, 2004. Available from: <http://public.itrs.net/Files/2004UpdateFinal/2004Update.htm>]. The interconnect system of this one billion transistor chip will provide the required high-speed signal and power to transmit each transistor on the chip. This system will deliver high frequency signals to various circuits, and the parasitic effects associated with interconnect will become evident and cannot be ignored. Small parasitic capacitance (*C*) between interconnect are required to reduce the crosstalk, power consumption, and RC delay associated with the metal interconnect system. Therefore, interconnect with low dielectric constant (*k*) materials is required.

In this study, hydrogen silsesquioxane (HSQ) thin films prepared under various conditions are employed as the intermetal dielectric and the high frequency characteristics of Al–HSQ system are investigated and compared with those of Al–SiO_2 system. The *S*-parameters of the Al interconnect are measured for insertion loss and crosstalk noise. The interconnect transmission parameters are extracted from the *S*-parameters. A figure of merit (FOM) is employed to evaluate the characteristics of the Al–HSQ system at high frequencies (100 MHz–20 GHz). It is found that Al interconnect with HSQ films annealed at 400 °C has an insertion loss of 1.64 dB/mm, a coupling of −13.3 2 dB at 20 GHz, and a propagation delay of 0.121 ps/μm, while those of the PECVD SiO_2 films are 2.01 dB/mm (insertion loss), −13.40 dB (coupling), and 0.149 ps/μm (propagation delay). The Al-400 °C-annealed-HSQ system has better performance than the Al–SiO_2 system does from 100 MHz to 20 GHz. However, specimens with 350 °C-annealed HSQ films or plasma-treated HSQ films exhibit larger insertion losses and higher crosstalk noises than those with PECVD SiO_2 films do. Both annealing temperature and O_2 plasma treatment of the HSQ films affect the high frequency characteristics of the Al–HSQ system.

Keywords: *S*-parameters; High speed interconnect; Hydrogen silsesquioxane; Coupling effect; Attenuation noise; Insertion loss; Low-*k* dielectric; Crosstalk

1. Introduction

As the dimensions of ULSI circuits shrink, there is a need for faster performance and higher circuit density. Multilayer interconnect structures are the trend to produce high-density circuits and enhance device performance. However, at high operational frequencies (>1 GHz), the parasitic effects associated with the multilayer interconnect become a limiting factor for chip performance and can not be ignored [1–3].

The parasitic effects of the multilayer interconnect are comprised of resistance with variation due to the skin effect at high frequencies, the self- and mutual-inductance of interconnects, the shunt capacitances from signal lines to ground lines, the parasitic capacitance resulted from the intermetal dielectric, the leakage of the dielectric material and substrate, etc. All result in signal distortion, propagation delay,

* Corresponding author. Tel.: +886 3 5731927; fax: +886 3 5724361.
E-mail addresses: doubles.ee89g@nctu.edu.tw (C.-C. Ho), bschiou@mail.nctu.edu.tw (B.-S. Chiou).
[1] Tel.: +886 3571212154203; fax: +886 35131590.

0167-9317/$ - see front matter © 2005 Elsevier B.V. All rights reserved.
doi:10.1016/j.mee.2005.12.006

and crosstalk noise [3–9]. In order to retain signal integrity at high frequencies, the requirements for the intermetal dielectric include: a small dielectric constant, low leakage current, low moisture absorption, adequate mechanical strength, simplicity of process, and ease of integration [10–16].

Hydrogen silsesquioxane (HSQ) is a potential candidate of which the dielectric constant can be further reduced by forming a highly porous three-dimensional network structure [16]. The general formula for HSQ is $(HSiO_{1.5})_{2n}$, $n = 2$, 3, etc., which is an inorganic material that can be considered as a derivative of SiO_2 in which one of the four oxygen atoms bonded to every silicon atom is replaced by hydrogen. However, HSQ has many integration issues, such as: thermal dissociation of Si–H bonds, oxidation, plasma damage, formation of –OH bonds, absorption of water, etc. [11–13]. It was reported that with appropriate plasma treatments the thermal stability of HSQ could be enhanced [12]. Nevertheless, the plasma treatment may damage the surface and/or change the surface chemistry of HSQ and the reliability of the low-k dielectric HSQ may degrade [11–13].

In this work, HSQ films are prepared and O_2 plasma treatments are applied to some specimens. The electrical properties of Al interconnect on HSQ (Al/HSQ/thermal SiO_2/Si) and Al interconnect on SiO_2 (Al/PECVD SiO_2/thermal SiO_2/Si) are measured and compared. The electrical parameters (R, L, C, and G) are extracted from the measured S-parameters. The signal transient characteristics with signal delays and crosstalk noises between adjacent interconnect lines are evaluated by the inverse Fourier transform.

2. Experimental procedures

Four inch diameter p-type (1 0 0) Si wafers with nominal resistivity of 5–10 Ω cm were used as substrate. After standard RCA cleaning, a 100 nm SiO_2 film was grown on the Si substrate. Two dielectrics, hydrogen silsesquioxane (HSQ) and SiO_2, were deposited on top of the SiO_2/Si substrate. Hydrogen silsesquioxane (HSQ) was prepared by spin-coating Dow-Corning Flowable Oxide (FOX) on the wafer and then baked at 150, 250, and 350 °C for 1 min. Annealing was performed in N_2 furnace from 350 to 400 °C for 60 min as described previously [13]. The thickness of HSQ is about 500 nm after annealing. Some samples were subjected to plasma treatment. The O_2 plasma was operated at a pressure of 40 Pa for 5 min, a plasma power of 100 W and a chamber temperature of 250 °C. The amorphous SiO_2 films, deposited by the decomposition of tetraethyl orthosilicate, with 500 nm in thickness were deposited with PECVD (Multichamber PECVD, STS-MULTIPLEX CLUSTER SYSTEM, England) at 300 °C (substrate temperature) and 200 W. Then, 500 nm Al films were deposited by thermal evaporation onto the dielectric material to serve as interconnect.

The imizidation and chemical bonds structure of HSQ films were investigated by Fourier transform infrared reflection-absorption spectrometer (FT–IR–RAS). The FT–IR–RAS system used in this study (DA8.3, Bomen Inc., Canada) was a stand-alone measurement system. Its beam was P-polarized incident beam, and scan mode was 75° grazing incident angle reflectance because the samples were thin films. Two hundred scans were carried out, and the resolution was $\sim$1 cm^{-1}. A field emission scanning electron microscope (FESEM, S-4000, Hitachi Ltd., Japan) was used to examine the microstructure of the films. An LCR meter (HP-4285, Hewlett–Packard Co., USA) was employed to measure the capacitance and the dissipation factor of the dielectric from 75 kHz to 2.5 MHz. A Network Analyzer (HP-85122A, Hewlett–Packard Co., USA) which operates from 100 MHz to 20 GHz was used to measure the S-parameters of the interconnect on-wafer with the microwave probes. Before each measurement, the calibrations were carried out with SOLT pads (short, open, load, and through) purchased from Cascade Microtech (Cascade Microtech, USA). A de-embedding method proposed in [17] was employed to deduct the shunt parasitics of the probing pads. Then, the signal transient characteristics with signal delays and crosstalk noises between adjacent interconnect lines are evaluated by the inverse Fourier transform from S-parameters of the interconnect.

3. Results and discussion

3.1. Dielectric properties and microstructures of the HSQ films

A typical structure of HSQ is an Si–O cage containing Si–H bonds. The three-dimensional network structure of HSQ is obtained through annealing process. After annealing, some of the Si–H bonds dissociate and the cage is rearranged into network structure as shown schematically in Fig. 1(a) [13,18]. Fig. 1(b) shows the Fourier transform infrared (FT–IR) spectra before and after annealing with or without O_2 plasma treatment. The spectra exhibit a Si–H peak at 2250 cm^{-1}, Si–O stretching cage-like peak at 1130 cm^{-1}, Si–O stretching network peak at 1070 cm^{-1}, Si–O bending cage-like peak at 863 cm^{-1} and Si–O bending network peak at 830 cm^{-1} as listed in Fig. 1(a) [11]. Datum in the brackets in Fig. 1(b) is the relative Si–H peak area with respect to the Si–H peak area of the as-deposited HSQ films. The Si–H bond (2250 cm^{-1}) absorbance decreases as annealing temperature increases especially after O_2 plasma treatment. The Si–O stretching cage-like bond (1130 cm^{-1}) and Si–O bending cage-like bond (863 cm^{-1}) break to form Si–O stretching network bond (1070 cm^{-1}) and Si–O bending network bond (830 cm^{-1}), respectively. Fig. 1(c) indicates that the absorbance peak ratios of Si–O network bonds (830 and 1070 cm^{-1}) to Si–O cage-like bonds (863 and 1130 cm^{-1}) are almost constant when specimens are annealed at temperatures less than or equal to 300 °C, while the increases in peak ratios are observed

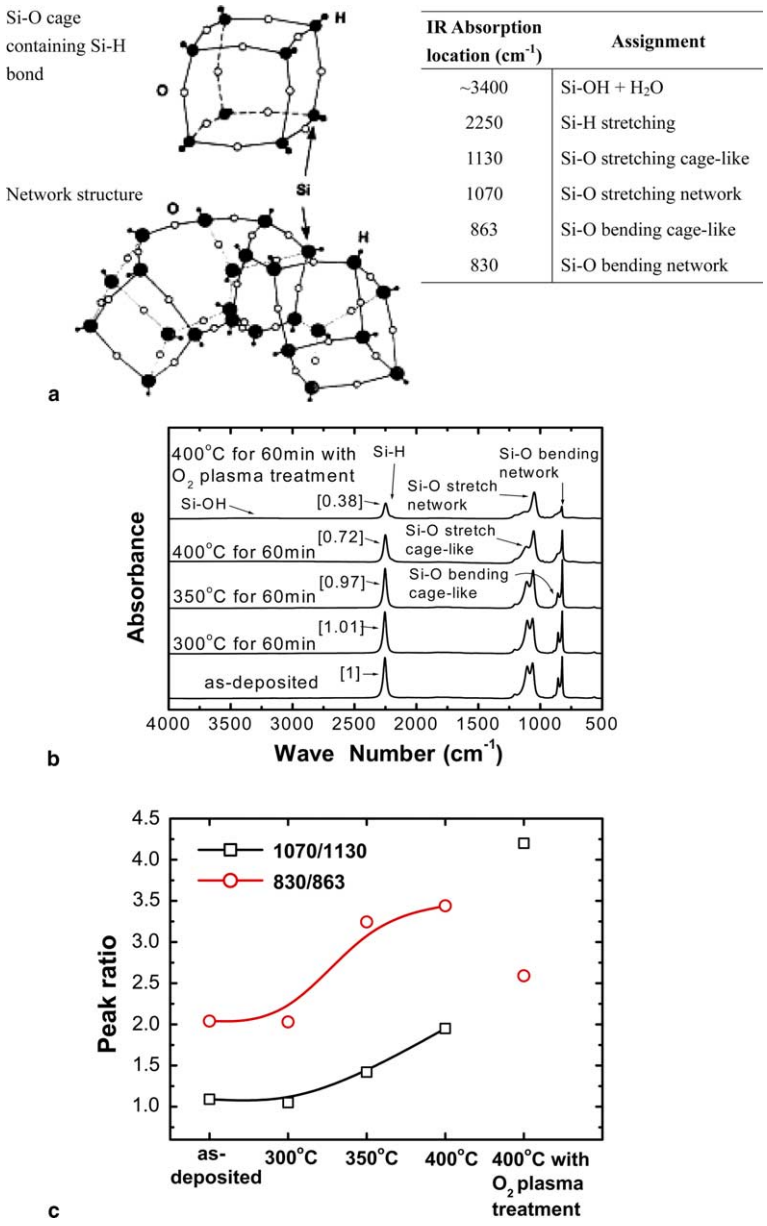

IR Absorption location (cm^{-1})	Assignment
~3400	Si-OH + H_2O
2250	Si-H stretching
1130	Si-O stretching cage-like
1070	Si-O stretching network
863	Si-O bending cage-like
830	Si-O bending network

Fig. 1. (a) Schematic diagram of the structure of hydrogen silsesquioxane (HSQ) and infrared absorption assignments applicable to HSQ films [11,13,18]. (b) FT–IR spectra of HSQ films before and after annealing. Datum in the brackets is the relative Si–H peak area with respect to the Si–H peak area of the as-deposited HSQ films. (c) Absorbance peak ratio of Si–O network bond to Si–O cage-like bond of HSQ films annealed at various temperatures for 60 min. As listed in (a), the IR location of Si–O network bonds are 830 and 1070 cm^{-1}, while those of Si–O cage-like bonds are 863 and 1030 cm^{-1}.

after annealing at 350 °C and above. This suggests that the structure of HSQ changes from cage-like structure to network structure after it was annealed at above 350 °C for 60 min.

Fig. 2(a) gives the dielectric constant (k) and dissipation factor (DF) as functions of frequency from 75 kHz to 2.5 MHz. The k values are 2.5, 2.4, and 3.4 for HSQ annealed at 350, 400, and 400 °C with O_2 plasma treatment, respectively. The SEM photographs, shown in Fig. 2(b)–(d), indicate that films annealed at 400 °C with and without plasma treatment have denser surface than those annealed at 350 °C which have a porosity of ~12%. The absorption of moisture via the open pores is the major cause for the larger k and DF of the 350 °C-annealed sample as compared to those of the 400 °C-annealed ones.

Oxygen plasma bombardment raises the k value of the 400 °C-annealed HSQ from 2.4 to 3.4. The FT–IR spectra (Fig. 1(b)) indicate a drop in the Si–H absorbance after plasma treatment. Our previous study indicates that exposure to the O_2 plasma causes the breaking of Si–H bonds, and this leads to the formation of dangling bonds that absorb water rapidly when the HSQ is exposed to air after the O_2 plasma treatment [13]. Hence, an increase in the dielectric constant is observed.

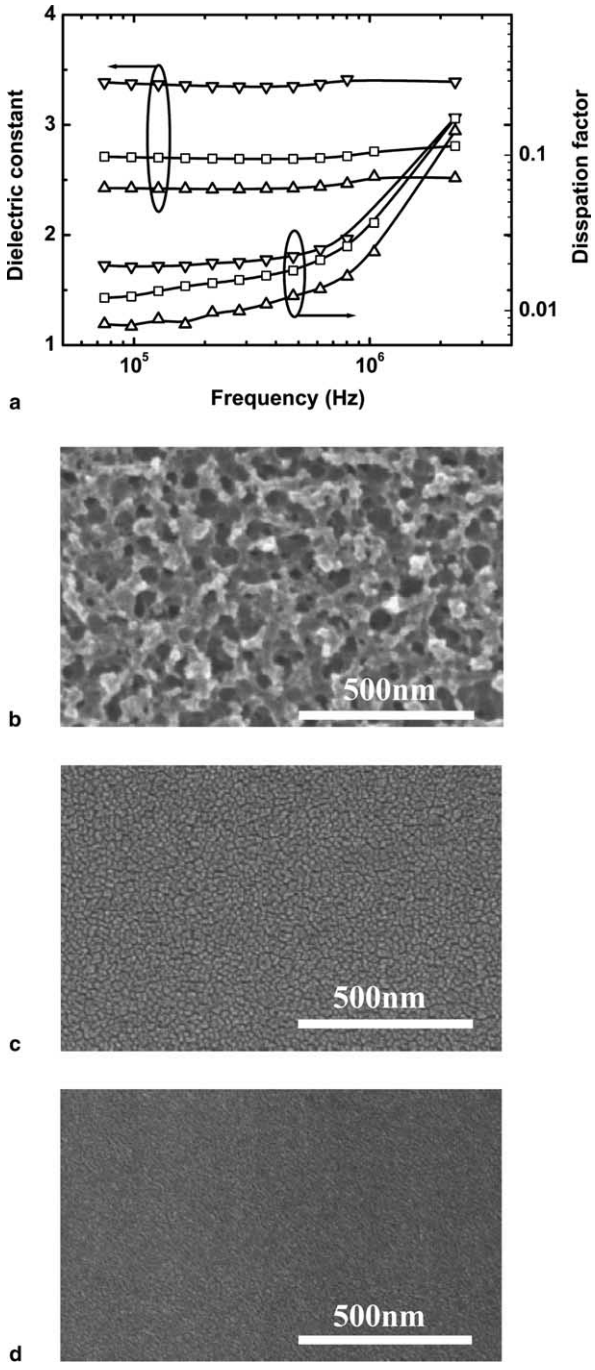

Fig. 2. (a) Dielectric constant and dissipation factor of HSQ versus frequency after 350 °C (□), 400 °C (△) annealing for 60 min and 400 °C annealing for 60 min followed by O_2 plasma treatment for 5 min (▽); (b) the SEM photograph of 350 °C-annealed HSQ films; (c) the SEM photograph of 400 °C annealed HSQ films; and (d) the SEM photograph of 400 °C annealed HSQ films with O_2 plasma treatment.

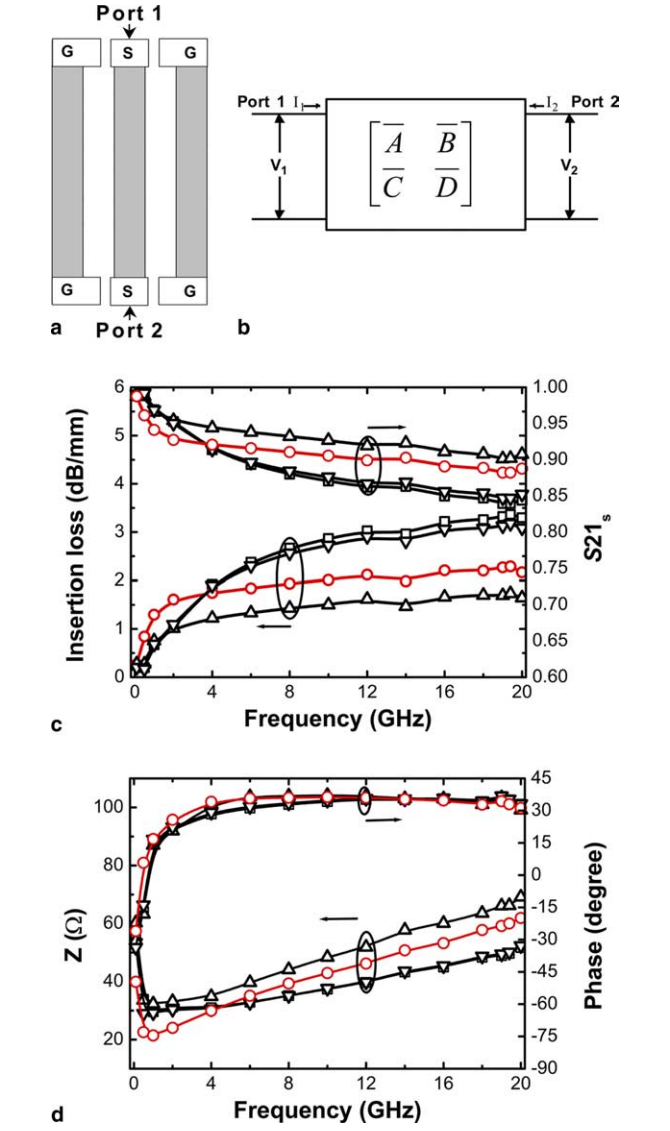

Fig. 3. (a) Schematic diagram of the interconnect structure for insertion loss measurement (interconnect length is 400 μm, spacing is 100 μm, and width is 50 μm in this case). (b) A two-port network of the interconnect structure shown in (a). (c) Insertion loss and *S*-parameter $S21_s$ as functions of frequency. (d) Magnitude (Z) and phase of impedance of the transmission lines as functions of frequency of specimens with HSQ films annealed at 350 °C (□), 400 °C (△), and 400 °C followed by O_2 plasma treatment (▽), and PECVD SiO_2 films (○).

3.2. Insertion loss

The test structure for insertion loss measurement has one signal line as exhibited in Fig. 3(a). With the ground-signal-ground probes, insertion loss (dB/mm) is obtained from the *S*-parameters $S21_s$ and $S\,11_s$ where the subscript s denotes one signal line

$$\text{Insertion loss} = 10 \times \log[|S21_s|^2/(1-|S11_s|^2)]/\text{length} \quad (\text{dB/mm}) \tag{1}$$

A two-port network with a 2×2 transmission matrix as shown in Fig. 3(b) is defined for the test structure

$$\begin{bmatrix} V_1 \\ I_1 \end{bmatrix} = \begin{bmatrix} \overline{A} & \overline{B} \\ \overline{C} & \overline{D} \end{bmatrix} \times \begin{bmatrix} V_2 \\ I_2 \end{bmatrix} \tag{2}$$

Specimens with 400 °C-annealed HSQ dielectric have the smallest insertion loss, i.e. the largest $S21_s$, among all the specimens studied. However, O_2 plasma treatment increases the insertion loss of the interconnect, as shown

in Fig. 3(c). Fig. 3(d) gives the magnitude and phase of the characteristic impedance of the transmission line as functions of frequency. The magnitude of impedance initially decreases and then increases with the increase of frequency. The phase of impedance varies from negative (capacitive) to positive values (inductive) at ~1 GHz where a resistive characteristic impedance ranging from 21.4 Ω (specimens with PECVD SiO_2) to 32.3 Ω (specimens with the 400 °C-annealed HSQ) is obtained. The insertion loss does not become smaller as the magnitude of the characteristic impedance approaches 50 Ω (i.e. the characteristic impedance of the cable for *S*-parameters measurement) because the transmission line becomes inductive.

3.3. Extraction of interconnect transmission parameters

The transmission matrix can be expressed in terms of the interconnect parameters (*R*, *L*, *C*, *G*) of the equivalent circuit given in Fig. 4(a)

$$\begin{bmatrix} \overline{A} & \overline{B} \\ \overline{C} & \overline{D} \end{bmatrix} = \begin{bmatrix} 1 & \frac{R}{2} \\ 0 & 1 \end{bmatrix} \times \begin{bmatrix} 1 & \frac{j\omega L}{2} \\ 0 & 1 \end{bmatrix} \times \begin{bmatrix} 1 & 0 \\ j\omega C & 1 \end{bmatrix} \times \begin{bmatrix} 1 & 0 \\ G & 1 \end{bmatrix} \times \begin{bmatrix} 1 & \frac{j\omega L}{2} \\ 0 & 1 \end{bmatrix} \times \begin{bmatrix} 1 & \frac{R}{2} \\ 0 & 1 \end{bmatrix} \tag{3}$$

Hence:

$$\overline{A} = 1 + j\left(\frac{j\omega L + R}{2}\right)\omega C + G\left(\frac{j\omega L + R}{2}\right), \tag{4}$$

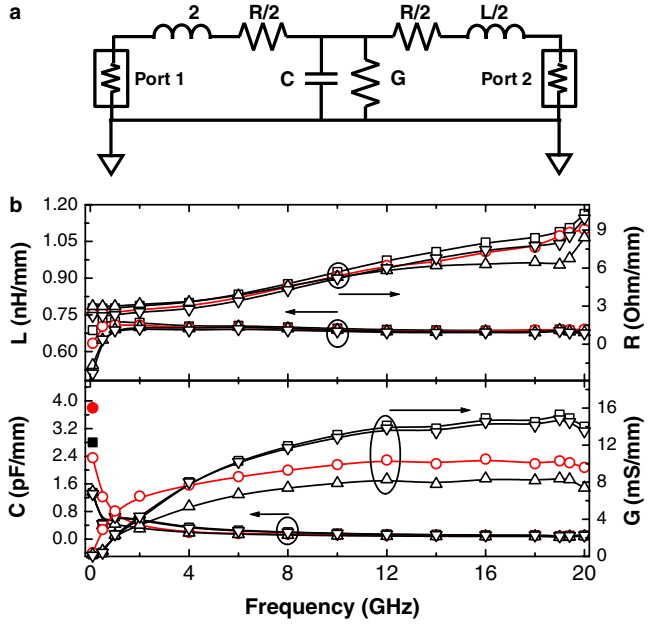

Fig. 4. (a) Equivalent circuit model of the interconnect structure shown in Fig. 3(a). (b) Extracted interconnect parameters: capacitance (*C*), conductance (*G*), inductance (*L*), and resistance (*R*), as functions of frequency of specimens with HSQ films annealed at 350 °C (□), 400 °C (△), and 400 °C followed by O_2 plasma treatment (▽), and PECVD SiO_2 films (○). (■) and (●) are the measured 100 kHz capacitances of HSQ and SiO_2, respectively.

$$\overline{B} = \frac{j}{4}(j\omega LG + GR + 4 + \omega^2 LC - j\omega CR)(\omega L - jR), \tag{5}$$

$$\overline{C} = G + j\omega C, \tag{6}$$

$$\overline{D} = 1 + j\left(\frac{j\omega C + G}{2}\right)\omega L + R\left(\frac{G + j\omega C}{2}\right), \tag{7}$$

where ω is angular frequency, and *R*, *L*, *C*, and *G* are resistance, inductance, capacitance, and conductance per unit length of the interconnect, respectively.

The relationship between the measured *S*-parameters and the transmission matrix is [19]

$$\begin{bmatrix} \overline{A} & \overline{B} \\ \overline{C} & \overline{D} \end{bmatrix} = \begin{bmatrix} \frac{(1+S_{11})(1-S_{22})+S_{12}S_{21}}{2S_{21}} & Z_0\frac{(1+S_{11})(1+S_{22})-S_{12}S_{21}}{2S_{21}} \\ \frac{(1-S_{11})(1-S_{22})-S_{12}S_{21}}{2Z_0S_{21}} & \frac{(1-S_{11})(1+S_{22})+S_{12}S_{21}}{2S_{21}} \end{bmatrix}, \tag{8}$$

where Z_0 equals to 50 Ω which is the characteristic impedance of the cable used in this study. The interconnect parameters *R*, *L*, *C*, and *G* are then derived on the basis of Eqs. (4)–(8) from the measured *S*-parameters and are exhibited in Fig. 4(b). Specimens with 400 °C-annealed HSQ have the smallest conductance *G*, however, plasma treatment raises the *G* of the 400 °C-annealed HSQ. Previous work indicates that exposure to the O_2 plasma causes Si–H bonds to break. The breaking of Si–H bonds leads to the formation of dangling bonds which absorb water rapidly to form Si–OH bonds when the HSQ is exposed to air after the O_2 plasma treatment [13]. Hence, an increase in the conductance after plasma treatment is observed as shown in Fig. 4(b).

The resistances *R* of the interconnect increase with the increase of frequency. Skin effect is the major reason which causes the increase of *R* with frequency. The thickness of the Al interconnect is 500 nm. The skin depth (δ), defined as $\delta = 1/(\pi\mu\sigma f)^{0.5}$, is around 603 nm for a 20 GHz signal propagating through Al interconnect. The interconnect inductance, resulted from magnetic flux enclosed between the signal line and the return path, is dependent on the space to the return path and is relatively constant over frequency.

The capacitance of the dielectrics decreases with increasing frequency as expected from the polarization mechanisms of the dielectrics. However, the drop in the capacitance exceeds what one would normally expect from polarization mechanisms alone. The dielectric constant *k* of SiO_2 at optical frequency (~10^{14} Hz) is 2.25 which is about 57% of that of the static region ($k \sim 4$ at 100 kHz [20]). As shown in Fig. 4(b), the 100 kHz capacitances are 3.8 and 2.8 pF/mm for SiO_2 and 400 °C-annealed HSQ, respectively. While the 10 GHz capacitances are 0.10 pF/mm (SiO_2) and 0.08 pF/mm (400 °C-annealed HSQ). The measured capacitances at higher frequencies drop to about 2.7% of those at low frequency (100 kHz). This is beyond what one would expect from polarization mechanisms alone. It is argued that the abrupt decrease of *C* is due to changes of the interconnect propagation mode.

There are three propagation modes for metal-insulator-semiconductor (MIS) transmission lines: (1) skin effect mode which occurs at high frequency (>100 MHz) and low substrate resistivity (<0.01 Ωcm), the substrate behaves like a lossy conductor. Hence, the magnetic field and electric field penetrate only the insulator. (2) Dielectric Quasi-TEM mode which occurs at frequencies higher than the dielectric relaxation frequency of Si substrate, the semiconductor substrate acts like a dielectric, such that the electric field and magnetic field can penetrate into the semiconductor substrate. (3) Slow wave mode which occurs when the operating frequency is low compared to the dielectric relaxation frequency and the substrate resistivity is moderate, the substrate acts like neither of the above. Only the magnetic field can penetrate into substrate because skin depth is larger than the thickness of the substrate, while electric field can penetrate only into the insulator [4,21–24].

In this study, the characteristic frequency of slow wave mode is about 50 MHz (f_o) and the dielectric relaxation frequency of the Si substrate (f_e) is about 15 GHz. The signal propagation will transit from slow wave mode to Quasi-TEM mode at frequencies ranged from 15 MHz ($0.3f_o$) to 22.5 GHz ($1.5f_e$). This may be the major reason for the abrupt drop of the capacitance at about 1 GHz as shown in Fig. 4(b).

The delay times, that is, time to 50% of the input signal, are 291 and 359 ps for specimens with 400 °C-annealed HSQ and SiO_2, respectively, as shown in Fig. 5. The interconnect length is 2400 μm. Hence, the propagation delays of Al-400 °C-annealed HSQ and Al–SiO_2 are 0.121 and 0.149 ps/μm, respectively. Signal attenuation is observed as the steady-state output is about 98% of the input signal.

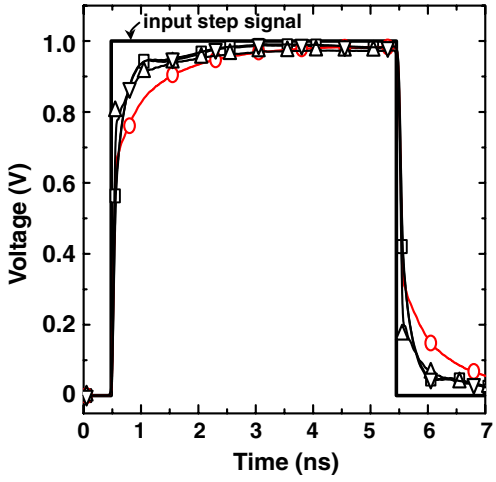

Fig. 5. Signal transient response of the interconnect structure shown in Fig. 3(a) with HSQ films annealed at 350 °C (□), 400 °C (△), and 400 °C followed by O_2 plasma treatment (▽), and PECVD SiO_2 films (○). The interconnect length is 2400 μm.

3.4. Crosstalk noise

Crosstalk noises between two interconnect lines are measured with the test structure shown in Fig. 6(a) where signal is applied to the aggressor line (*S*1) and coupling

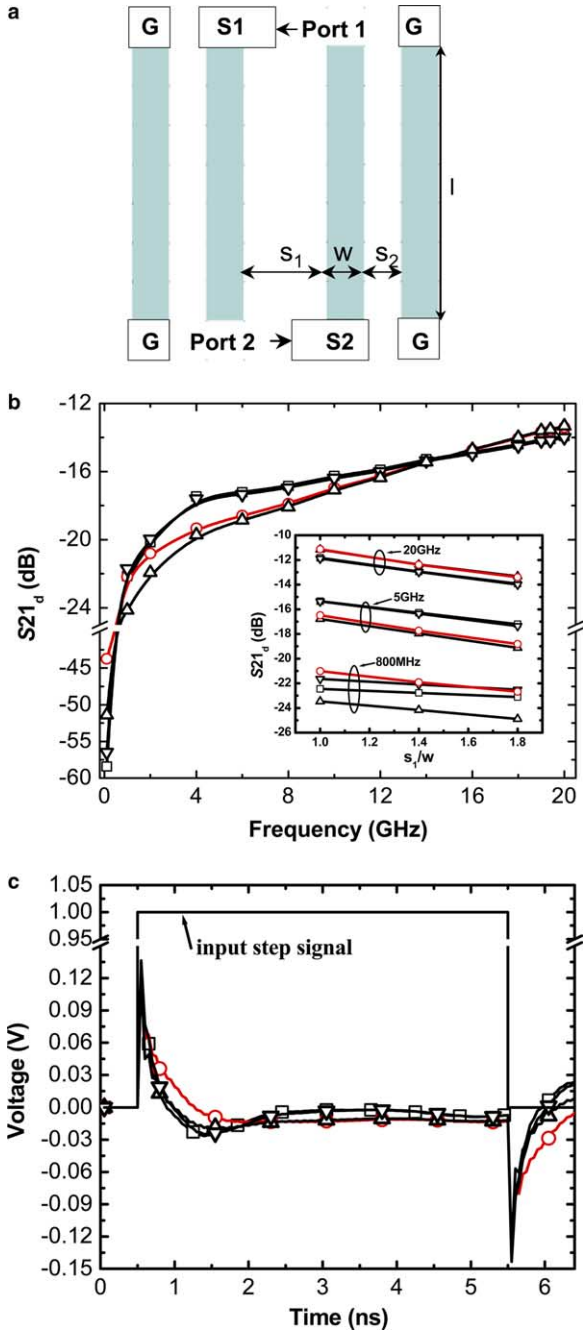

Fig. 6. (a) Schematic diagram of the interconnect structure for crosstalk measurements with two signal (*S*) lines and two ground (*G*) lines. The ends of the signal lines are open. Length $l = 400$ μm, spacing $s_1 = 90$, 70, or 50 μm, $s_2 = 30$ μm, and width $w = 50$ μm. (b) $S21_d$ as a function of frequency, and the inset is the frequency dependence of $S21_d$ as a function of s_1/w ratio. (c) Transient voltage across the victim line (*S*2) when a step signal is applied to the aggressor line (*S*1). The dielectric films are HSQ films annealed at 350 °C (□), 400 °C (△), and 400 °C followed by O_2 plasma treatment (▽), and PECVD SiO_2 films (○), respectively.

voltage across the victim line ($S2$) is measured. The S-parameter ($S21_d$) is employed to evaluate the coupling between the two lines. As exhibited in Fig. 6(b), $S21_d$ increases with the increase of frequency, and specimens with the 400 °C-annealed HSQ films have the lowest $S21_d$ at frequencies below 15 GHz. While those with 350 °C-annealed HSQ films and 400 °C-annealed HSQ films followed by O_2 plasma treatment show less coupling at higher frequencies (>15 GHz). Increasing the spacing/width ratio of the interconnect decreases the coupling as seen in the inset of Fig. 6(b). The transient voltages of the victim line are evaluated by the inverse Fourier transform when a step voltage is applied to the aggressor interconnect. As exhibited in Fig. 6(c), specimens with 400 °C-annealed HSQ films have a smallest transient peak (i.e. crosstalk noise) of 0.121 V. The transient peaks are 0.136, 0.136, and 0.130 V, for specimens with 350 °C-annealed HSQ films, 400 °C-annealed HSQ films followed by O_2 plasma treatment, and PECVD SiO_2, respectively. The first transient peak is mainly caused by capacitive coupling, and the following oscillations are attributed to both capacitive and inductive coupling.

3.5. Trade off between signal attenuation and crosstalk noise

As mentioned previously, among the specimens studied, samples with 400 °C-annealed HSQ have the smallest signal attenuation and crosstalk noise from 100 MHz to 15 GHz. However, at frequencies above 15 GHz, less coupling is observed for specimens with 350 °C-annealed HSQ or O_2 plasma-treated HSQ. A figure of merit (FOM) is thus defined to evaluate the high frequency performance of the interconnect on the basis of both signal attenuation and crosstalk noise

$$\mathrm{FOM} = |S21_s| \times (1 - |S21_d|) \tag{9}$$

The larger $S21_s$ (the smaller signal attenuation) and the smaller $S21_d$ (the smaller crosstalk), the larger the FOM. As exhibited in Fig. 7, specimens with 400 °C-annealed HSQ films show the largest FOM over the range of 100 MHz to 20 GHz among all the specimens studied.

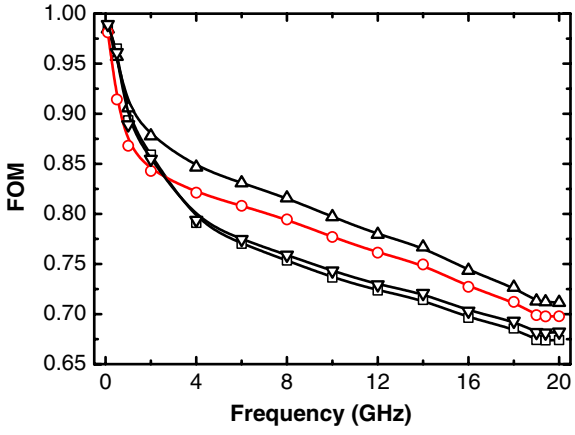

Fig. 7. Figure of merit (FOM) as a function of frequency of specimens with HSQ films annealed at 350 °C (□), 400 °C (△), and 400 °C followed by O_2 plasma treatment (▽), and PECVD SiO_2 films (○).

4. Conclusions

Hydrogen silsesquioxane (HSQ) films prepared under various conditions were integrated with Al interconnects. The dielectric constant of HSQ films annealed at 400 °C is smaller than those of HSQ films annealed at 350 °C or subjected to O_2 plasma bombardment. The SEM photographs and FT–IR spectra suggest that absorption of water via open pores or by dangling bonds cause the increase of the dielectric constant. The high frequency characteristics of the Al-HSQ system are studied and compared to those of the Al–SiO_2 system on the basis of the measured S-parameters. The interconnect transmission parameters R, L, C, and G, are extracted from the S-parameters. It is found that specimens with 400 °C-annealed HSQ have the smallest conductance (G) and O_2 plasma treatment raises the G of the 400 °C- annealed HSQ. The increase of resistance (R) with increasing frequency is attributed to skin effect. The interconnect inductance (L) is relatively constant over the frequency range of the measurement. However, dramatic drop in capacitance is observed at ~1 GHz. The characteristic frequency of slow wave mode and the dielectric relaxation frequency of the Si substrate in this study are 50 MHz and 15 GHz, respectively. It is believed that change of the interconnect propagation mode causes the abrupt decrease of C. The Al–HSQ system with 400 °C-annealed HSQ exhibits smaller insertion loss, lower crosstalk noise, and smaller signal propagation delay than the Al–SiO_2 system does.

Acknowledgment

This work is sponsored by National Science Council, Taiwan, under the contract number NSC 93-2216-E-009-023.

References

[1] Semiconductor Industry Associations, International Technology Roadmap for Semiconductors, 2004. Available from: <http://public.itrs.net/Files/2004UpdateFinal/2004Update.htm>.
[2] P. Heydari, S. Abbaspour, M. Pedram, in: Proceedings of the International Conference on VLSI Design, 2002, pp. 132–137.
[3] S.S. Wong, P. Yue, R. Chang, S.Y. Kim, B. Kleveland, F. O'Mahony, in: Proceedings of the International Symposium on Quality Electronic Design, 2003, pp. 1–6.
[4] J.S. Ko, B.K. Kim, K. Lee, IEEE Trans. Electron Dev. 44 (1997) 856–861.
[5] Y. Eo, W.R. Eisenetadt, IEEE Trans. Adv. Pack. 26 (2003) 392–401.
[6] J.K. Wee, Y.J. Park, H.S. Min, D.H. Gho, M.H. Seung, H.S. Park, IEEE Trans. Microw. Theory Tech. 46 (1998) 1346–1443.
[7] Y. Eo, W.R. Eisenstadt, J. Shim, IEEE Trans. Adv. Pack. 23 (2000) 470–479.
[8] S.H. Choi, K. Roy, in: Proceedings of the First IEEE International Workshop on Electronic Design, Test and Applications, 2002, pp. 365–369.

[9] A. Deutsch, G.V. Kopcsay, P.J. Restle, H.H. Smith, G. Katopis, W.D. Becker, P.W. Coteus, C.W. Surovic, B.J. Rubin, R.P. Dunne, T. Gallo, K.A. Jenkins, L.M. Terman, R.H. Dennard, G.A. Sai-Halasz, B.L. Krauter, D.R. Knebel, IEEE Trans. Microw. Theory Tech. 45 (1997) 1836–1844.
[10] K. Char, B.J. Cha, S. Kim, in: Proceedings of the International Interconnect Technology Conference, 2004, pp. 219–221.
[11] P.T. Liu, T.C. Chang, Y.L. Yang, S.M. Sze, IEEE Trans. Electron Dev. 47 (2000) 1733–1739.
[12] P.T. Liu, T.C. Chang, S.M. Sze, F.M. Pan, Y.J. Mei, W.F. Wu, M.S. Tsai, B.T. Dai, C.Y. Chang, F.Y. Shih, H.D. Huang, Thin Solid Films 332 (1998) 345–350.
[13] C.T. Chen, B.S. Chiou, J. Mater. Sci. Mater. Electron. 15 (2004) 139–143.
[14] H.S. Tzeng, B.S. Chiou, W.F. Wu, C.C. Ho, J. Electron. Mater. 33 (2004) 796–801.
[15] C.T. Chen, B.S. Chiou, J. Electron. Mater. 33 (2004) 368–373.
[16] S.P. Jeng, K. Taylor, T. Seha, M.C. Chang, J. Fattaruso, R.H. Havemann, in: Proceedings of the Symposium on VLSI Technology Digest of Technical Papers, 1995, pp. 61–62.
[17] H. Cho, D.E. Burk, IEEE Trans. Electron Dev. 38 (1991) 1371–1375.
[18] M.J. Loboda, C.M. Grove, R.F. Schneider, J. Electrochem. Soc. 145 (1998) 2861–2866.
[19] D.M. Pozar, Microwave Engineering, second ed., Wiley, New York, 1998.
[20] C.C. Ho, B.S. Chiou, J. Mater. Sci. Mater. Electron., submitted for publication.
[21] H. Hasegawa, M. Furukawa, H. Yanai, IEEE Trans. Microw. Theory Tech. MTT-19 (1971) 869–881.
[22] Y.R. Kwon, V.M. Hietala, K.S. Champlin, IEEE Trans. Microw. Theory Tech. MTT-35 (1987) 545–551.
[23] Y. Eo, W.R. Eisenetadt, IEEE Trans. Compon. Hybr. Manufact. Technol. 16 (1993) 555–562.
[24] W.R. Eisenetadt, Y. Eo, IEEE Trans. Compon. Hybr. Manufact. Technol. 15 (1992) 483–490.